# A New Method for Simulating Gaseous Cookoff on Short Bounded Domains

Haran Jackson[a,**], Nikos Nikiforakis[a]

[a]*Cavendish Laboratory, JJ Thomson Ave, Cambridge, UK, CB3 0HE*

**Abstract**

In this study, an Arrhenius reaction model is combined with the GPR model of continuum mechanics [45, 17] and the feasibility of simulating cookoff within this framework is demonstrated. A new method is then proposed for significantly accelerating the simulation of slow cookoff on short, bounded domains. The acoustic components of the system are approximated by assuming that the pressure equilibrates on a faster time scale than the other processes of the system, and only a reduced subsystem is solved. This development is assessed numerically and shown to be effective.

The GPR model is able to describe both solids and fluids (viscous and inviscid, Newtonian and non-Newtonian) in the same framework, with thermal conduction. It should be well suited to simulating cookoff, where multiple materials and phases of matter may be present, and current models rely on coupling different sets of equations to describe the different materials. The hyperbolicity of the GPR system also makes it amenable to large-scale parallelisation, and it does not suffer from the appearance of nonphysical infinite-speed waves, unlike the parabolic Navier-Stokes equations, or the classical Fourier law of heat conduction.

*Keywords:* Cookoff, GPR

**Contents**



To Do:

- Read Clarke & Cant method of determining onset
- Find way of defining "fast" and "slow" cookoff
- Sort out spikes in concentration

## 1. Background

### *1.1. Cookoff*

The term “cookoff” is used to denote the process by which explosives deflagrate or detonate unintentionally, due to ambient heat from the surrounding environment. It is imperative that this process is properly understood, to avoid repeats of the many fatal and destructive civil and military accidents that have occurred over the years.

Cookoff is extremely complicated, with many different stages. Many different materials and phases may be present at the

*Corresponding author
**Principal corresponding author
*Email address:* hj305@cam.ac.uk (Haran Jackson)

same time. Large costs, difficulty in experimental design, and safety issues mean that computational modeling has become of paramount importance in predicting the cookoff behavior of different materials in different scenarios. Computational modeling presents a whole new set of challenges, however.

Despite extensive algorithmic optimization, computational techniques such as adaptive mesh refinement, and a roughly 1000-fold increase in maximum attained computing power between 2006 and 2016 (~100 TFlop/s - ~100PFlop/s [2]), cookoff simulations remain relatively computationally challenging. As detailed by Asay [5], we are still a long way from being able to perform accurate large-scale simulations of the full systems of equations governing such phenomena on less than a time scale on the order of days. It is noted that computational error is linearly dependent on domain size, and CPU time depends non-linearly. Thus an increase of 3 orders of magnitude in computational power yields only a tenfold decrease in error in 2D simulations, and a decrease of only 5.6 times in 3D. There is a clear need for new fundamentally-different ways of reducing the computational effort required.

If the time step of the computational method used to model cookoff is restricted by a CFL condition based on the speed of sound, the heating phase will take an excessively long time to calculate, even though the dominating process is thermal conduction; a slow, smooth process. A strict CFL condition will be required to accurately resolve the deflagration/detonation phase, but this phase represents a small fraction of the total time. There have been several attempts to circumvent this issue, described here.

Selesovský [54] models the thermal loading of explosives using the Frank-Kamenetskii model of thermal conduction with Arrhenius reaction kinetics [18] (disregarding the non-conductive features of the process, such as flow and acoustics). The time step in the heating phase is chosen according to a standard stability condition according to the parabolic nature of the system. Once thermal runaway occurs, the time step is reduced by an amount obtained through trial-and-error (building upon results from Sućeska and Matečić-Mušanić [56]) ensuring that the latter stages of the process are resolved correctly. This reduction is not actually required for numerical stability; it is required for accuracy. Clearly, it is not desirable to obtain the time step experimentally for every reactive process one wishes to model.

A huge amount of the work on cookoff modeling has been performed at the Lawrence Livermore (and to a lesser extent, Sandia) National Laboratories. Much of the work at LLNL has gone into their ALE3D multiphysics code [1]. One of the methods employed in the ALE3D code to circumvent the time step restriction in the heating phase is variable mass scaling. Implemented by Yoh et al. [64, 65, 63], this technique is based on the work of Prior [46]. The system is integrated explicitly and the density of the materials in the system is scaled higher so as to reduce the effective speed of sound, and thus artificially increase the time step permitted by the standard CFL condition. In practice, the desired time step is fixed and the density is scaled to its required value. At the transition between the heating and combustion phases, the scaling is reduced incrementally to its natural value. Despite its success in increasing the computational efficiency of the calculations - especially when inertia effects are negligible - this technique appears to have fallen out of favor in recent years in simulations involving large amounts of fluid flow, owing to the associated spurious oscillations in the motions of the heated materials detailed by Howard et al. [30]. It is still used in more static thermal heating problems (see for example Khairallah and Anderson [35], who obtain a 3- to 10-fold speed up using this method).

Lately, a different method has been used by Nichols and Schofield [43] and McClelland et al. [39]. In the heating phase, the fluid is modeled with the incompressible Navier-Stokes equations, which are solved using the semi-implicit pressure projection method presented by Gresho [26, 25]. This removes the stringent CFL condition based on the speed of sound. Although each iteration is more computationally taxing, much larger time steps can be taken than with an explicit solution method. At each step, the advection of the reactive species is calculated with an explicit forward Euler scheme and its diffusion is calculated with an implicit backward Euler scheme. Only one iteration of both of these schemes is performed at each step, meaning that the time step for all processes is in fact limited by a CFL condition based on the velocity of the fluid. These velocities tend to be small in slow cookoff situations, leading to a large time step at this stage. $C_{cfl} = 0.1$ was used in the cited studies. The system governing the chemical reaction is also iterated at each time step.

In the early stages of the simulation the aforementioned method is efficient, but as the material heats up the time step will reduce to the point that it is faster to perform a full explicit calculation at each step. This was determined experimentally in [43] to occur roughly when the implicit time step is less than 100 times larger than the explicit time step. A complex transition to the explicit solver is then undertaken. Neighboring nodal values for the chemical composition are linearly interpolated to give element-centered values. The density and internal energy are found iteratively from the average fluid pressure, the averaged temperature, and the compositional state. This is done as inconsistencies in these variables can be introduced in the preceding stages. The velocity field can become chaotic under the implicit solver so this is set to zero everywhere. Owing to the complexity of the transition, the CFL time step is reduced by a factor of 1000 to allow local equilibration of the system and to avoid any macro-scale aberrations.

This transition process introduces large changes to the system at the most critical point in determining its subsequent violent evolution. The time of transition and the time step reduction factor have to be set by trial-and-error, meaning that they may need to be tested for each new simulation set-up. A process of this sort will always be necessary, however, if the heating phase is solved implicitly. In addition to the schemes outlined here, in [39] the diffusivity of the species was artificially increased (by trial-and-error) to avoid numerical instabilities. The fluid viscosity was also increased ten-fold to slow the flow and increase the time step given by the velocity CFL condition on the

advection of the species. Clearly, adjustments such as these are not desirable.

The method presented in this study seeks to resolve the issues detailed here, at least in the physical situations to which it is applicable (discussed in Section 3). The same mathematical model is used in all stages of the cookoff process, and the choice of solvers in the early and late stages does not necessitate a complex reconciliation of state variables at transition. The transition point is identified using an objective measure, ensuring that no trial-and-error studies are required to ascertain empirical parameters governing the transition process (as required by some extant methods). While overcoming these issues, the new method still provides a significant computational speedup, as discussed in Section 4.4.

### *1.2. Parabolic vs Hyperbolic Systems*

Information in parabolic systems of partial differential equations travels at infinite speed, and a perturbation in the condition of the system at one point has an effect at all other points instantaneously. Thus, parabolic systems (such as the Navier-Stokes equations or the classical Fourier equations of heat transfer) are not amenable to parallelisation. By contrast, solutions to hyperbolic systems are wave-like in structure, with finite speeds of propagation of information. Solutions on different parts of the domain can be calculated independently, leveraging the great advances that have been made recently in parallel computing technologies, particularly in the burgeoning field of general purpose GPU computing. The use of hyperbolic models also allows for the utilization of Riemann solvers, on which there has been a great deal of work over the years (see Toro [58] for a broad overview).

Even disregarding the practical benefit of employing hyperbolic schemes, there is the more profound issue that we live in a causal universe, and ultimately parabolic systems cannot be a "true" description of reality. Although this discrepancy often does not matter in practice, there are problems to which parabolic models are particularly unsuited (see [20, 24, 23, 15] among many others).

In addition to the problems already discussed, in the case of the Navier-Stokes formulation in particular, the stress tensor is derived from empirical observation of the macroscopic behavior of steady, homogeneous flows, rather than from a first-principles microscopic description. As shown by Yakhot [62], this can result in problems when modeling essentially unsteady and non-equilibrium flow. On top of this, the NS equations are second order, making them more sensitive to the quality of the computational mesh than a first order system.

Several attempts to produce a hyperbolic formulation of viscous fluid dynamics have been made (see for example [8, 21, 23, 31, 42, 44, 49]). However, as noted by Peshkov and Romenski [45], the systems described all essentially take the following form for some model-specific dissipative quantity $X$:

$$\dot{X} = -\frac{1}{\beta}\left(X - X_{NS}\right) \tag{1}$$

where $\beta$ is a relaxation parameter and $X_{NS}$ is the value obtained from the Navier-Stokes equations. This is a hyperbolic relaxation model, constructed as a first-order extension to the second order NS equations.

These models are all based on the series expansion of the distribution function with respect to a set of moments. The physical meanings of the moments are largely ignored, and they have neither microscopic counterparts, nor are they defined as volume-averaged quantities. Additionally, a naive model of the form above is not frame invariant. Often this is remedied by introducing an objective stress rate $\dot{X}$, but as this can be defined in many ways, this results in different solutions to the model, along with violation of the second law of thermodynamics and loss of well-posedness of the initial value problem [45].

The recently proposed model of Peshkov and Romenski benefits from the advantages of hyperbolicity, while avoiding the deficits inherent in the existing hyperbolic models. It is derived fundamentally from a microscopic description of the continuum phenomena it describes. It is also able to model different materials and phases of matter in the same framework. This feature makes it well-suited to simulating the process of cookoff.

### *1.3. The Model of Godunov, Peshkov and Romenski*

The GPR model, first introduced by Peshkov and Romenski [45] and expanded upon by Dumbser et al. [17], takes the following form:

$$\frac{\partial \rho}{\partial t} + \frac{\partial \left(\rho v_k\right)}{\partial x_k} = 0 \tag{2a}$$

$$\frac{\partial \left(\rho v_i\right)}{\partial t} + \frac{\partial (\rho v_i v_k + p\delta_{ik} - \sigma_{ik})}{\partial x_k} = 0 \tag{2b}$$

$$\frac{\partial A_{ij}}{\partial t} + \frac{\partial \left(A_{ik} v_k\right)}{\partial x_j} + v_k\left(\frac{\partial A_{ij}}{\partial x_k} - \frac{\partial A_{ik}}{\partial x_j}\right) = -\frac{\psi_{ij}}{\theta_1(\tau_1)} \tag{2c}$$

$$\frac{\partial \left(\rho J_i\right)}{\partial t} + \frac{\partial \left(\rho J_i v_k + T\delta_{ik}\right)}{\partial x_k} = -\frac{\rho H_i}{\theta_2\left(\tau_2\right)} \tag{2d}$$

$$\frac{\partial \left(\rho s\right)}{\partial t} + \frac{\partial \left(\rho s v_k + H_k\right)}{\partial x_k} = \frac{\rho}{\theta_1\left(\tau_1\right) T}\psi_{kl}\psi_{kl} + \frac{\rho}{\theta_2\left(\tau_2\right) T} H_k H_k \tag{2e}$$

where $\theta_1$ and $\theta_2$ are positive scalar functions, and $\psi = \frac{\partial E}{\partial A}$ and $\boldsymbol{H} = \frac{\partial E}{\partial \boldsymbol{J}}$. Entropy does not decrease during the dissipative time evolution:

$$\frac{\partial \left(\rho s\right)}{\partial t} + \frac{\partial \left(\rho s v_k + H_k\right)}{\partial x_k} \geq 0 \tag{3}$$

(2e) can be replaced with the following equation, which will be used instead when solving the model in this study:

$$\frac{\partial \left(\rho E\right)}{\partial t} + \frac{\partial \left(\rho E v_k + \left(p\delta_{ik} - \sigma_{ik}\right) v_i + q_k\right)}{\partial x_k} = 0 \tag{4}$$

Note that (2a), (2b), (2c), (2d), (4) can be written in the following form:

$$\frac{\partial \boldsymbol{Q}}{\partial t} + \boldsymbol{\nabla} \cdot \boldsymbol{F} + \boldsymbol{B} \cdot \nabla \boldsymbol{Q} = \boldsymbol{S} \tag{5}$$

The following definitions are given:

$$p = \rho^2 \frac{\partial E}{\partial \rho} \tag{6a}$$

$$\sigma = -\rho A^T \frac{\partial E}{\partial A} \tag{6b}$$

$$T = \frac{\partial E}{\partial s} \tag{6c}$$

$$\boldsymbol{q} = \frac{\partial E}{\partial s} \frac{\partial E}{\partial \boldsymbol{J}} \tag{6d}$$

To close the system, the EOS must be specified, from which the above quantities and the sources can be derived. $E$ is the sum of the contributions of the energies at the molecular scale (microscale), the material element[1] scale (mesoscale), and the flow scale (macroscale):

$$E = E_1(\rho, s) + E_2(A, \boldsymbol{J}) + E_3(\boldsymbol{v}) \tag{7}$$

In this study, $E_1$ is taken to correspond to an ideal or stiffened gas:

$$E_1 = \frac{p + \gamma p_\infty}{(\gamma - 1)\rho} \tag{8}$$

where $p_\infty = 0$ for an ideal gas. The temperature is given by:

$$T = \frac{p + p_\infty}{(\gamma - 1) c_v \rho} \tag{9}$$

and the speed of sound by:

$$c_0 = \sqrt{\frac{\gamma (p + p_\infty)}{\rho}} \tag{10}$$

$E_2$ is chosen to have the following quadratic form:

$$E_2 = \frac{c_s^2}{4} \|\mathrm{dev}(G)\|_F^2 + \frac{\alpha^2}{2} \|\boldsymbol{J}\|^2 \tag{11}$$

$\alpha$ is a constant related to the characteristic velocity of propagation of heat waves:

$$c_h = \frac{\alpha}{\rho} \sqrt{\frac{T}{c_v}} \tag{12}$$

[1]The concept of a *material element* corresponds to that of a fluid parcel from fluid dynamics, applied to both fluids and solids.

$G = A^T A$ is the Gramian matrix of the distortion tensor, and $\mathrm{dev}(G)$ is the deviator (trace-free part) of $G$:

$$\mathrm{dev}(G) = G - \frac{1}{3} \mathrm{tr}(G) I \tag{13}$$

$E_3$ is the usual specific kinetic energy per unit mass:

$$E_3 = \frac{1}{2} \|\boldsymbol{v}\|^2 \tag{14}$$

The following forms are chosen:

$$\theta_1(\tau_1) = \frac{\tau_1 c_s^2}{3 |A|^{\frac{5}{3}}} \tag{15a}$$

$$\theta_2(\tau_2) = \tau_2 \alpha^2 \frac{\rho T_0}{\rho_0 T} \tag{15b}$$

$$\tau_1 = \frac{6\mu}{\rho_0 c_s^2} \tag{16a}$$

$$\tau_2 = \frac{\rho_0 \kappa}{T_0 \alpha^2} \tag{16b}$$

The justification of these choices is that classical Navier–Stokes–Fourier theory is recovered in the stiff limit $\tau_1, \tau_2 \to 0$ [17]. This results in the following relations:

$$\sigma = -\rho c_s^2 G\, \mathrm{dev}(G) \tag{17a}$$

$$\boldsymbol{q} = \alpha^2 T \boldsymbol{J} \tag{17b}$$

$$-\frac{\psi}{\theta_1(\tau_1)} = -\frac{3}{\tau_1} |A|^{\frac{5}{3}} A\, \mathrm{dev}(G) \tag{17c}$$

$$-\frac{\rho \boldsymbol{H}}{\theta_2(\tau_2)} = -\frac{T \rho_0}{T_0 \tau_2} \boldsymbol{J} \tag{17d}$$

The following constraint also holds [45]:

$$\det(A) = \frac{\rho}{\rho_0} \tag{18}$$

The model as presented here has its roots in Godunov and Romenski's 1970s model of elastoplastic deformation [22]. The two models are very similar in structure. The differences lie in the physical interpretation of $A$, the appearance of algebraic source terms in the evolution equations for $A$, and the inclusion of thermal conduction by the evolution of $\boldsymbol{J}$. Whereas the earlier model described only solids, the new model seeks to describe fluids as well. In the former, $A$ was viewed as describing the global deformation of the medium; it is now regarded as describing the local deformability of the material elements comprising the medium, containing information about their rotation and deformation. Unlike in previous continuum models, material elements have not only finite size, but also internal structure.

The strain dissipation time $\tau_1$ of the GPR model is a continuous analogue of Frenkel's "particle settled life time" [19]; the characteristic time taken for a particle to move by a distance of the same order of magnitude as the particle's size. Thus, $\tau_1$ characterizes the time taken for a material element to rearrange with its neighbors. $\tau_1 = \infty$ for solids and $\tau_1 = 0$ for inviscid fluids. It is in this way that the GPR model seeks to describe all three major phases of matter, as long as a continuum description is appropriate for the material at hand.

The evolution equation for $\boldsymbol{J}$ and its contribution to the energy of the system are derived from Romenski's model of hyperbolic heat transfer, originally proposed in [37, 52] and implemented in [51, 50]. In this model, $\boldsymbol{J}$ is effectively defined as the variable conjugate to the entropy flux, in the sense that the latter is the derivative of the specific internal energy with respect to $\boldsymbol{J}$. Romenski remarks that it is more convenient to evolve $\boldsymbol{J}$ and $E$ than the heat flux or the entropy flux, and thus the equations take the form given here. $\boldsymbol{J}$ can intuitively be thought of as a thermal analogue of momentum. $\tau_2$ characterizes the speed of relaxation of the thermal impulse due to heat exchange between material elements.

### *1.4. Modeling Reactive Processes*

In this study, when modeling reactive gases, the following equation is introduced alongside (2a), (2b), (2c), (2d), (4):

$$\frac{\partial(\rho\lambda)}{\partial t} + \frac{\partial(\rho\lambda v_k)}{\partial x_k} = -\rho\lambda K(T) \tag{19}$$

$K$ is the rate of reaction - a function of temperature, whose form depends on the type of reaction kinetics used. The EOS (7) is modified to include:

$$E_r(\lambda) = -Q_c(1-\lambda) \tag{20}$$

In discrete ignition temperature reaction kinetics, no reaction occurs below the ignition temperature, $T_i$. Above $T_i$, the reaction proceeds at a constant rate $K_0 > 0$:

$$K(T) = \begin{cases} K_0 & T \geq T_i \\ 0 & T < T_i \end{cases} \tag{21}$$

A more sophisticated model of reaction kinetics was devised by Svante Arrhenius in 1889 [4, 3]:

$$K(T) = B_c e^{-E_a/(R_c T)} \tag{22}$$

where $B_c$ is some pre-exponential (with units of frequency), and $E_a$ is the activation energy of the reactive species. Often, the system is characterized by the dimensionless inverse activation energy:

$$\epsilon = \frac{R_c T_0}{E_a} \tag{23}$$

## 2. Numerical Methods

The GPR model, being non-conservative, with stiff source terms, represents a particularly challenging set of PDEs. In this study they are solved by an ADER-WENO method. First, the cell-wise constant state variable data from the current time step is reconstructed using high-order spatial polynomials according to the WENO method. This reconstruction is then extended to a reconstruction in both space and time for each individual cell in the domain, using the Discontinuous Galerkin method. A finite volume solver is then used to couple neighboring cells and produce the cell-wise constant data at the next time step. In this study, all simulations were performed in 1D. The methods presented here are extensible to higher dimensions, however (see [17, 9]).

### *2.1. Time Step and Boundary Conditions*

Let $\Lambda_i^n$ be the set of eigenvalues of the GPR system evaluated at $\boldsymbol{Q_i^n}$. $C_{cfl} < 1$ is a constant (usually taken to be 0.9, unless the problem being simulated is particularly demanding, requiring a lower value). The eigenvalues determine the speed of propagation of information in the solution to the Riemann Problem at the cell interfaces, and the time step is chosen to ensure that the characteristics do not enter into other cells between $t_n$ and $t_{n+1}$:

$$\Delta t_n = \frac{C_{cfl} \cdot \Delta x}{\max_i \left|\Lambda_i^n\right|} \tag{24}$$

Transmissive boundary conditions (allowing material and heat to pass through) are implemented by setting the state variables in the boundary cells to the same value as their non-boundary neighbors. Reflective boundary conditions are implemented in the same way, except that the directions of the velocity and thermal impulse vectors in the boundary cells are reversed. Where fixed temperature boundary conditions are used, reflective boundary conditions are first imposed, after which the pressure is altered so that the boundary cell has the desired temperature $T_{fixed}$:

$$p = \rho(\gamma - 1) c_v T_{fixed} - p_\infty \tag{25}$$

Where a fixed boundary heat flux $q$ is specified, the quantity $\frac{q \cdot \Delta t}{\Delta x}$ is added to the value of $\rho E$ in the boundary cell. It may be appropriate to also fix $\boldsymbol{J}$ in the boundary cell in accordance with the specified heat flux (as $\boldsymbol{q} = \alpha^2 T \boldsymbol{J}$), but this was not done here, as no analogous procedure was undertaken in the studies with which this study compares its results. The effect of this measure is a potential area of further research.

### *2.2. Operator Splitting*

An operator splitting method is used when solving the reduced GPR system in slow cookoff simulations (detailed in Section 3). Take the following conservative hyperbolic system with sources:

$$\frac{\partial \boldsymbol{Q}}{\partial t} + \frac{\partial \boldsymbol{F}(\boldsymbol{Q})}{\partial x} = \boldsymbol{S}(\boldsymbol{Q}) \tag{26}$$

At time step $n$, using $\boldsymbol{Q^n}$ as initial data, the homogeneous system is evolved by time step $\Delta t$ to produce an intermediate state $\tilde{\boldsymbol{Q}}^{n+1}$:

$$\frac{\partial \boldsymbol{Q}}{\partial t} + \frac{\partial \boldsymbol{F}(\boldsymbol{Q})}{\partial x} = \boldsymbol{0} \tag{27}$$

There exist many methods with which to accomplish this (see Toro for an overview [58]). In this study, the following scheme is used:

$$\tilde{\boldsymbol{Q}}_i^{n+1} = \boldsymbol{Q}_i^n + \frac{\Delta t}{\Delta x}\left(\boldsymbol{F}_{i+\frac{1}{2}} - \boldsymbol{F}_{i-\frac{1}{2}}\right) \tag{28}$$

The subscript $i + \frac{1}{2}$ is used to denote the value between cells $i$ and $i + 1$. $\boldsymbol{F}_{i+\frac{1}{2}}$ was chosen to be the first-order First-Order Centered flux of Toro [59]:

$$\boldsymbol{F}_{i+\frac{1}{2}} = \frac{1}{2}\left(\boldsymbol{F}^{\boldsymbol{LF}}_{i+\frac{1}{2}} + \boldsymbol{F}^{\boldsymbol{RI}}_{i+\frac{1}{2}}\right) \tag{29}$$

where $\boldsymbol{F}^{\boldsymbol{LF}}_{i+\frac{1}{2}}$ is the Lax-Friedrichs flux:

$$\boldsymbol{F}^{\boldsymbol{LF}}_{i+\frac{1}{2}} = \frac{1}{2}\left(\boldsymbol{F}(\boldsymbol{Q}_i) + \boldsymbol{F}(\boldsymbol{Q}_{i+1})\right) + \frac{1}{2}\frac{\Delta x}{\Delta t}\left(\boldsymbol{Q}_i - \boldsymbol{Q}_{i+1}\right) \tag{30}$$

and $\boldsymbol{F}^{\boldsymbol{RI}}_{i+\frac{1}{2}}$ is the Richtmyer flux [48]:

$$\boldsymbol{Q}^{\boldsymbol{RI}}_{i+\frac{1}{2}} = \frac{1}{2}\left(\boldsymbol{Q}_i + \boldsymbol{Q}_{i+1}\right) + \frac{1}{2}\frac{\Delta t}{\Delta x}\left(\boldsymbol{F}(\boldsymbol{Q}_i) - \boldsymbol{F}(\boldsymbol{Q}_{i+1})\right) \tag{31a}$$

$$\boldsymbol{F}^{\boldsymbol{RI}}_{i+\frac{1}{2}} = \boldsymbol{F}\left(\boldsymbol{Q}^{\boldsymbol{RI}}_{i+\frac{1}{2}}\right) \tag{31b}$$

Next, $\tilde{\boldsymbol{Q}_i^{n+1}}$ is used as initial data to the following system of ODEs.

$$\frac{d\boldsymbol{Q}}{dt} = \boldsymbol{S}(\boldsymbol{Q}(t)) \tag{32}$$

This system is evolved by time step $\Delta t$ to produce $\boldsymbol{Q_i^{n+1}}$. There are many ways to achieve this, both analytical and numerical. Only analytical methods are used in this study, as described in the next section.

## 3. New Method for Simulating Cookoff

Take domain $x \in [0, L]$ with heating at the left boundary using either a fixed temperature or a fixed heat flux boundary condition, as described in Section 2.1. If the heating phase of the cookoff process (described in 1.1) takes time $t^*$, we require $L \ll c_0 \cdot t^*$. This requirement is explained in 5.1. The domain is initially occupied by a reactive fluid with concentration 1. The following technique accelerates the computation of the long heating phase.

Take the reactive thermal subsystem of the motionless reactive GPR model:

$$\frac{\partial(\rho J_i)}{\partial t} + \frac{\partial T}{\partial x_i} = -\frac{\rho H_i}{\theta_2(\tau_2)} \tag{33a}$$

$$\frac{\partial(\rho E)}{\partial t} + \frac{\partial q_k}{\partial x_k} = 0 \tag{33b}$$

$$\frac{\partial(\rho\lambda)}{\partial t} = -\rho\lambda K(T) \tag{33c}$$

$$E = \frac{p + \gamma p_\infty}{(\gamma - 1)\rho} + \frac{\alpha^2}{2}\|\boldsymbol{J}\|^2 - Q_c(1 - \lambda) \tag{34}$$

In [17] it is shown that the heat characteristic of this system has speed:

$$c_h = \frac{\alpha}{\rho}\sqrt{\frac{T}{c_v}} \tag{35}$$

It is also demonstrated that around equilibrium ($\boldsymbol{v} = \boldsymbol{0}$, $A = I$, $\boldsymbol{J} = \boldsymbol{0}$), the largest eigenvalue of the full GPR system has the following magnitude:

$$\sqrt{\frac{C\rho + \sqrt{C^2 - 4\rho^2 c_h^2\left(p + \frac{4}{3}c_s^2\right)}}{2\rho}}, \quad C = c_0^2 + c_h^2 + \frac{4}{3}c_s^2 \tag{36}$$

For example, with the conditions $\rho = 1$, $p = 1$ and parameters $c_s = 1$, $\alpha = 1$, $c_v = 2.5$, $\gamma = 1.4$ (as featured in many of the numerical tests in [17]), the heat characteristic has speed $c_h = \sqrt{\frac{2}{5}} \approx 0.632$, and the largest eigenvalue of the full system is approximately 2.20. Thus, by the definition in Section 2.1, the time step used in an explicit solver for the reduced system will be around 3.5 times larger than that for the full system. In this study, it is proposed that in simulating slow cookoff, the thermal subsystem alone is solved (similarly to the method employed in [38]). Unlike in the cited paper, however, the full reactive GPR system will be employed when the rate of the chemical reaction becomes critical, to capture the full dynamics of the violent combustion.

The chemical reaction is determined to be proceeding at a critical rate when the temperature curve leading away from the

heated boundary develops an inflection point. The rationale behind this criterion is that this phenomenon indicates that the chemical reaction has become the dominant heating process in the system, over the boundary heating. Points further away from the boundary are approaching temperatures close to the boundary temperature, leading to an inflection in the temperature curve.

The reduced system is still hyperbolic. Unlike the full system, however, it is also conservative. The ADER-WENO solver is no longer necessary, and a less expensive operator splitting scheme can be used, as described in Section 2.2. The homogeneous subsystem is solved to first order, as higher-order accuracy is not needed here, owing to the smooth dynamics of the heating process.

The ODE subsystem is:

$$\frac{dJ_i}{dt} = -\frac{\alpha^2}{\theta_2(\tau_2)} J_i \tag{37a}$$

$$\frac{d\lambda}{dt} = -K(T)\,\lambda \tag{37b}$$

$\rho$ is treated as constant in time in the reduced system and $p$ does not evolve over the time step of the ODE subsystem, so $T$ is constant over this period, giving the analytical solution:

$$J_i^{n+1} = \exp\left(-\frac{\alpha^2 \Delta t}{\theta_2(\tau_2)}\right) \tilde{J}_i^{n+1} \tag{38a}$$

$$\lambda^{n+1} = \exp\left(-K\left(\tilde{T}^{n+1}\right)\Delta t\right) \tilde{\lambda}^{n+1} \tag{38b}$$

The reduced system does not contain evolution terms for the density. It produces roughly the correct temperature profile, but $\rho$ remains static, with pressure given by $p = (\gamma - 1)\, c_v T \rho - p_\infty$. On the timescale produced by the slow heating rate, the pressure in the full system in fact tends to equilibrate across the domain quickly. A process is required to calculate $\rho, p$ correctly from $T$ in the reduced system.

$p$ is approximated as being spatially constant, and the velocity as $\mathbf{0}$. The velocity of the fluid in the heating phase is shown to have little effect on the combustive process in [39]. This is confirmed in Section 4.4, where the constant pressure assumption is also shown to work well. The average specific microscale energy in each cell is:

$$\overline{\rho E_1} = \frac{1}{n} \sum_i \rho_i \left( E_i - \frac{\alpha^2}{2} \|\boldsymbol{J}_i\|^2 + Q_c\,(1 - \lambda_i) \right) \tag{39}$$

Thus:

$$\bar{p} = (\gamma - 1)\,\overline{\rho E_1} - \gamma p_\infty \tag{40a}$$

$$\rho_i = \frac{\bar{p} + p_\infty}{(\gamma - 1)\, c_v T_i} \tag{40b}$$

Pressure and density are recalculated at every time step. This approximation is very computationally cheap, and works well under the circumstances investigated in Section 4.4. Not only is the time restriction based on the characteristic speeds of the system reduced, but the computational cost is reduced by solving a much smaller system.

In [17] it is shown that $c_s$ can be derived experimentally from:

$$c_s = \sqrt{\frac{3}{4}\left(c_\infty^2 - c_0^2\right)} \tag{41}$$

Similarly, it is suggested that $\alpha$ is derived experimentally by measuring $c_h$. Thus, the factor gain in the time step as a result of this procedure depends on the properties of the material being modeled, and may be significantly better or worse than the example value given here. Even in the worst-case scenario where the characteristics of the heat waves travel faster than those of the longitudinal pressure waves (and so there is not improvement in the time step), the computational cost is still greatly reduced.

For the purpose of this study, this procedure will be referred to as *the isobaric cookoff technique*.

## 4. Results

### 4.1. Viscous Shock-Induced Detonation

The GPR model is now combined with discrete ignition temperature reaction kinetics to model a ZND detonation wave[2] in a viscous, reactive, ideal gas. There is currently no published work in which the GPR model is integrated with a combustion model, and this test case serves to demonstrate that this combination reproduces well-established results.

The test consists of a Chapman-Jouget wave with speed 1, traveling into a region of totally unburnt gas. The initial conditions are taken from Helzel et al. [28]. On $x < 0.25$ we have $\rho = 1.4$, $p = 1$, $\boldsymbol{v} = \mathbf{0}$, $A = \sqrt[3]{1.4} \cdot I_3$, $\boldsymbol{J} = \mathbf{0}$, $\lambda = 0$. On $x \geq 0.25$ we have $\rho = 0.887565$, $p = 0.191709$, $\boldsymbol{v} = (-0.577350, 0, 0)$, $A = \sqrt[3]{0.887565} \cdot I_3$, $\boldsymbol{J} = \mathbf{0}$, $\lambda = 1$.

The material parameters are taken to be: $\gamma = 1.4$, $c_v = 2.5$, $\rho_0 = 1$, $p_0 = 1$, $c_s = 1$, $\alpha = 1$, $\mu = 10^{-4}$, $P_r = 0.75$, $Q_c = 1$, $K_0 = 250$, $T_i = 0.25$. The results for grids of 400 and 1600 cells at time $t = 0.5$ are found in Figure 1 on page 9. They are to be compared with those by Hidalgo and Dumbser [29]. The simulation with 400 cells corresponds well with that found

[2] Zel'dovich [66], von Neumann [60], and Döring [16] independently proposed this detonation model, whereby reactive gas is compressed to high pressure by an infinitely thin shock wave into a *von Neumann spike*, initiating the reaction. The reaction zone is located behind the spike. In the reference frame of the shock, the gas moves supersonically ahead of the shock, subsonically in the reaction zone, and sonically in the region behind the reaction zone (which is described by the Chapman-Jouget state [10, 33]. The energy released in the reaction is transported acoustically to the shock to support it.

in [29], and the simulation with 1600 cells is very close to Hidalgo's total variation diminishing reference solution calculated with 10,000 cells.

The von Neumann spike is well resolved, with the thin reaction zone behind it (corresponding to the region in which the concentration decreases from 1 to 0). The CJ state is maintained correctly behind the reaction zone. The spurious wave in the density is explained in [29] as being due to initialization errors occurring as a result of using exact algebraic conditions for an ideal (infinitely thin) CJ detonation wave, which are solved with a viscous model with finite reaction rate.

### *4.2. Heating-Induced Deflagration*

As a step towards modeling the slow cooking off problem, the GPR model is now applied to the situation presented by Clarke, Kassoy and Riley [11, 12, 13]. Here, the domain $x \in \left[0, 8.5 \times 10^{-6}\right]$ is occupied by an ideal gas with initial conditions $\rho = \rho_0 = 1.176$, $p = p_0 = 101325$, $\boldsymbol{v} = \mathbf{0}$, $A = I_3$, $\boldsymbol{J} = \mathbf{0}$ and material parameters $\gamma = 1.4$, $c_v = 718$, $c_s = 55$, $\alpha = 500$, $\mu = 1.98 \times 10^{-5}$, $P_r = 0.72$. These values are chosen to be similar to air at room temperature.

Thermal energy is added at the left boundary at a high power of $\frac{\gamma p_0 c_0}{P_r(\gamma-1)}$ (around $1.7\times10^8 Wm^{-2}$). The test is performed with both a combustible and an inert gas. In the former case, the initial concentration is set to $\lambda = 1$. Arrhenius reaction kinetics are used, with $Q_c = 6\gamma c_v T_0$, $B_c = 7 \times 10^{10}$, $\epsilon = \frac{1}{20}$. The subsequent evolutions of the systems for 400 cells are shown in Figure 2 on page 10. Nondimensionalized time and length variables $t^*, x^*$ are used, as in [12]:

$$t = \frac{\mu}{p_0 \gamma} t^* \tag{42a}$$

$$x = \frac{\mu c_0}{p_0 \gamma} x^* \tag{42b}$$

There are no analogues for $\alpha$ and $c_s$ in the models used by Clarke et al. $c_s$ is given the experimentally-derived value for $CH_3Cl$ at 30°C given in [17]. $\alpha$ is chosen so that the GPR results corresponded with those in [12]. The results presented here are thus close, but not identical to those of Clarke et al.

Note that heating the inert gas produces an acoustic wave of constant pressure, propagating ahead of the temperature curve. This pressure wave is also present in the heating of the combustible gas, where it proceeds in front of the combustion wave. The temperature increase accompanying this acoustic wave is not enough to ignite the reactive gas, and the thin reaction zone lags behind the acoustic wavefront. Although the combustion wave is referred to as a detonation wave in [12], it would now commonly be called a deflagration wave, as it travels subsonically and is not coincident with the shock wave. This phenomenon of a second, faster shock overtaking the combustion wave demonstrated experimentally by Kapila et al. [34], with a full mathematical analysis provided by Short [55], where it is shown to result from the steep temperature gradient at the time of ignition.

### *4.3. Heating-Induced Detonation*

It is now demonstrated that the heating-induced deflagration test can result in detonation if the temperature gradient upon ignition is less steep. This test is identical to the previous test, with one exception: $\epsilon$ is given the higher value of $\frac{1}{15}$. Thus, the activation energy is effectively lower, or equivalently, the whole gas volume is relatively closer to the ignition temperature when the gas at the left boundary ignites. The results of this test are shown in Figure 3 on page 11.

The von Neumann spike is present and well resolved, with a thin reaction zone appearing behind it in the concentration plot. Unlike in Section 4.1, the system does not relax to the CJ state behind the detonation wave, as thermal energy is continually added to the reflective left boundary. The region behind the reaction zone is thus complex.

### *4.4. Slow Cookoff*

The performance of the isobaric cookoff technique presented in Section 3 will now be investigated. The initial conditions for a combustible gas are taken from Section 4.2. There is a time-dependent fixed-temperature boundary condition on the left, as described in Section 2.1, and the right boundary is reflective. The temperature at the left boundary is given by $T = T_0\left(1 + t \cdot 10^6\right)$. Thus, this test can still be considered a quick cookoff in most contexts, but the heating process is four orders of magnitude slower than in the previous two tests; slow enough to demonstrate the isobaric cookoff technique.

Unlike in Section 4.2, as the heating rate is relatively low, the temperature gradient is fairly shallow at ignition, resulting in detonation rather than deflagration. The detonation wave reaches the end of the domain at about $t = 8.6 \times 10^{-7}$, with the long heating phase taking up most of this time. The detonation wave forms at around $8.5 \times 10^{-7}$. When using the isobaric cookoff technique, the full system is only calculated from around $t = 7 \times 10^{-7}$ onward.

The heating phase is shown in Figure 4 on page 12 at 9 equispaced points in time. The temperature profiles between the reduced and full system are very close. The constant pressure assumption works very well, as the heating rate is slow enough for the pressure differences it generates to equilibrate, and the domain is short enough that any acoustic waves emitted from the left boundary rebound into the domain. The pressure at each time step is slightly higher in the full system than the reduced system. This is due to the non-zero fluid velocities present in the full system (but not the reduced system) carrying heated material away from the left boundary, meaning that slightly more energy enters this system, as the boundary is held at a fixed, time-dependent value.

The zero velocities of the reduced system do not affect the shape of the final detonation wave, as the velocities in the full system are relatively small, but the indirect effect of this discrepancy

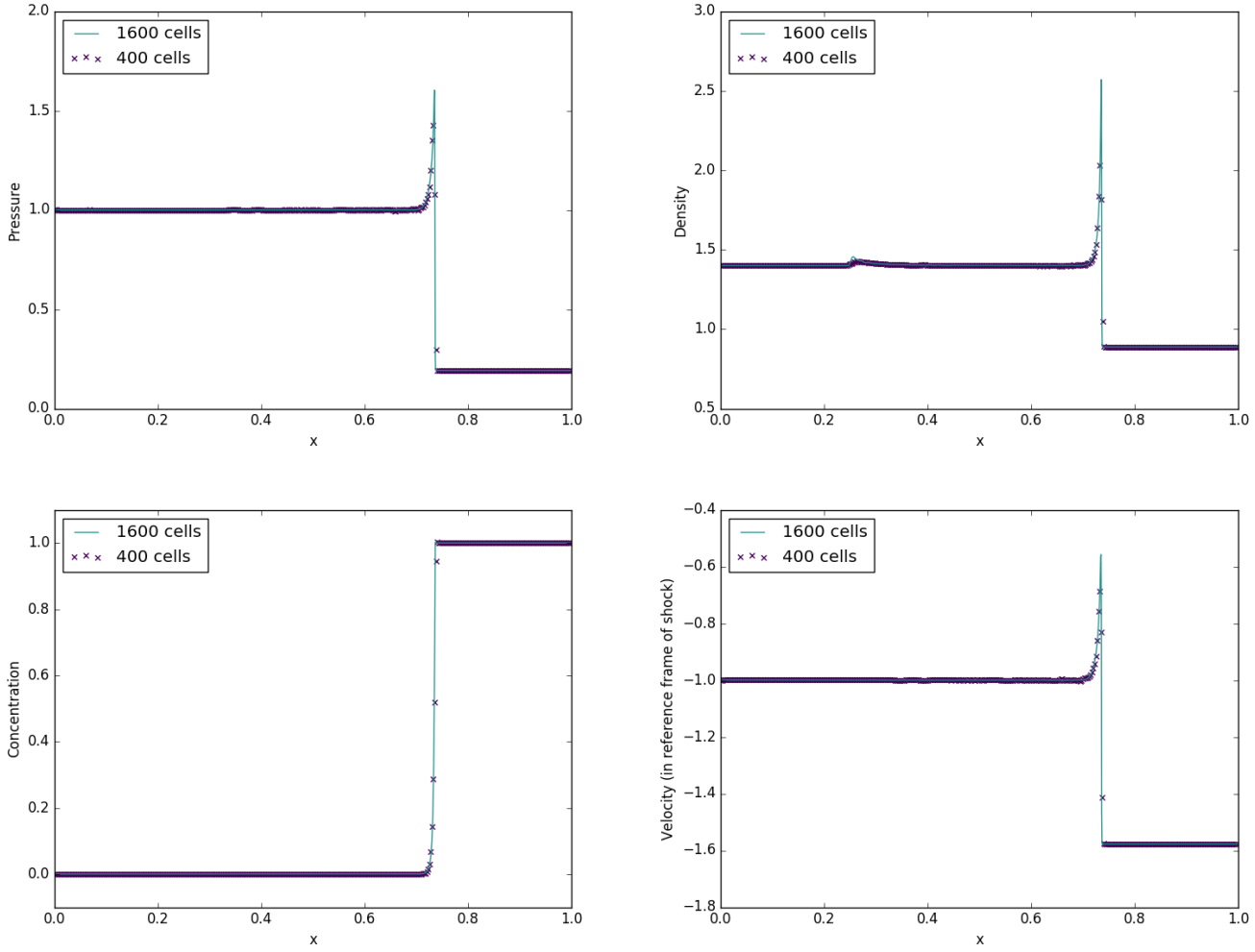


Figure 1: Pressure, density, concentration of reactant, and velocity (in the reference frame of the shock) in the viscous shock-induced detonation test

on the total energy of the system means that the reduced system detonates about $6.55 \times 10^{-9} s$ later than the full system[3]. The subsequent evolution of the systems are almost indistinguishable (see Figure 5 on page 13). Proposals to rectify the discrepancy in the total energies of the systems are discussed in 5.2.

During the heating phase, the average time step for the reduced system was $\Delta t = 5.758 \times 10^{-11}$, as opposed to $\Delta t = 4.447 \times 10^{-11}$ for the full system. This relatively small difference is attributed to the fact that the heat characteristics are relatively fast with the values of the material parameters used (chosen to match those used in the heating-induced deflagration test). However, the WENO, DG, and FV steps took on average 0.0703s, 0.8355s, and 0.9326s respectively per iteration of the full system. The operator splitting solver took on average 0.0001522s per iteration of the reduced system (a speed-up of over 4 orders of magnitude). In both cases, the auxiliary functions (such as those applying the boundary conditions) took on average 0.01547s per iteration[4]. Thus, the heating phase took a total of 25740s with the full system, and 168s with the reduced system (a roughly 150-fold speed-up). Of course, these results are very implementation- and hardware-specific, and alternative implementations, running on different platforms may yield different results.

## 5. Discussion

It has been demonstrated in Section 4.1, Section 4.2, and Section 4.3 that the GPR model coupled with Arrhenius reaction kinetics is capable of accurately modeling the deflagration and detonation phenomena required to simulate combustion. This system carries the benefits of being hyperbolic, as described in 1.2.

[3] Detonation is defined here as the point at which 2.5% of reactant in any cell has burned; a fairly arbitrary measure, to be discussed in 5.2.

[4] All times quoted here resulted from running a single-threaded implementation of the solver on an Intel Core i7 4910-MQ.

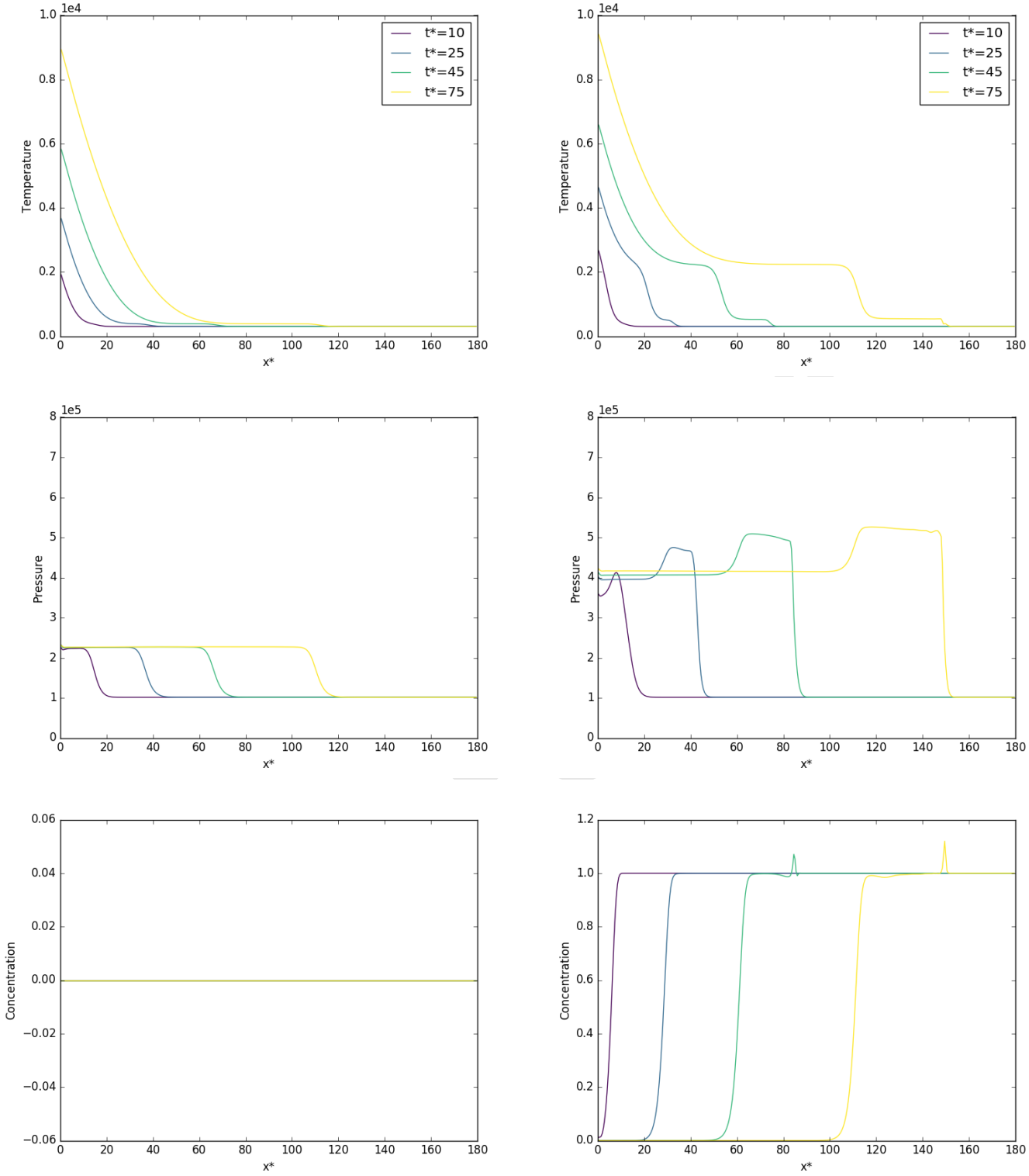


Figure 2: Temperature, pressure, and concentration of reactant in the heating-induced deflagration test with inert gas (left) / reactive gas (right)

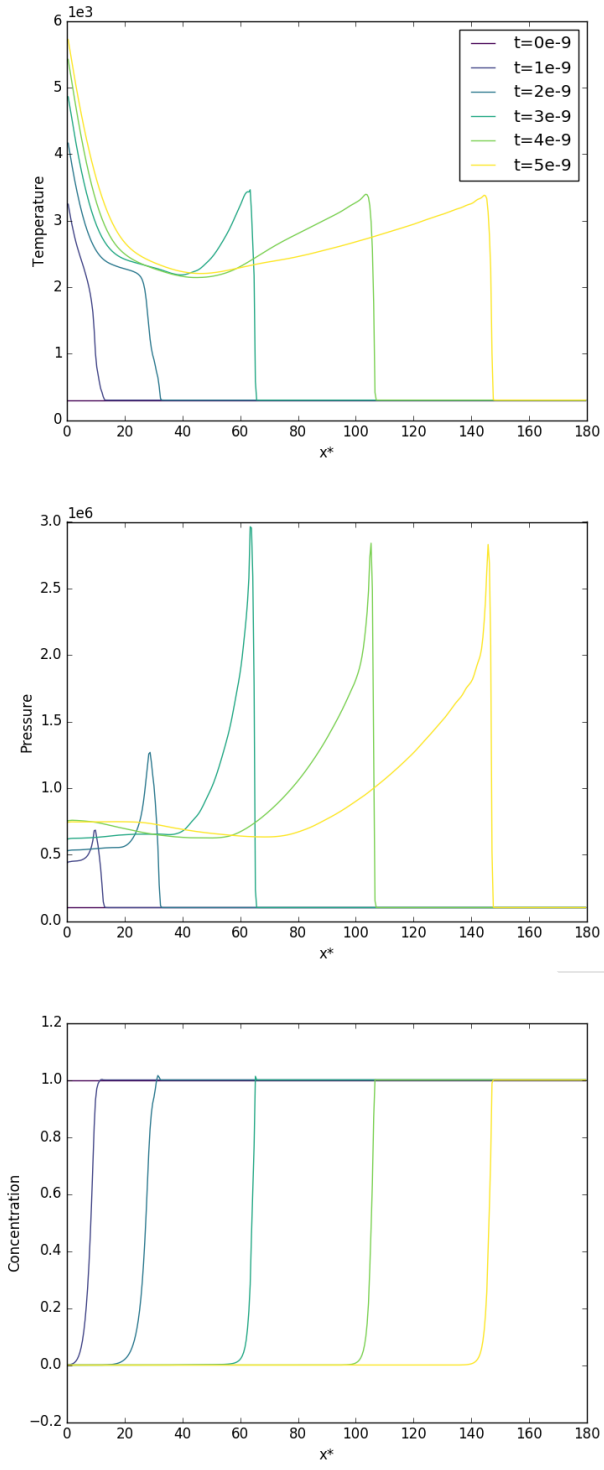


Figure 3: Temperature, pressure, and concentration of reactant in the heating-induced detonation test

The EOS used in this study was in every case either that of an ideal gas or a stiffened gas. Thus, solids could not be properly modeled. Although in the early days of cookoff simulation, generally only gases were considered, the focus now is very much on solids and the fluids that they interact with and produce over the course of the process. The isotropic hyperelastic EOS from [57] and the Mie-Grüneisen EOS are used with the GPR model in [9], providing some reference results against which to validate a future solid cookoff implementation. One outstanding problem regarding the GPR model is that of deriving a physically-relevant form of the function $\theta_1(\tau_1)$ that controls the evolution of the distortion tensor for each type of fluid or solid that one wishes to simulate. The form of $\theta_1$ used in this study works well for Newtonian fluids[5], but is not appropriate for non-Newtonian fluids (where rate of strain is not directly proportional to shear stress) [17]. As of the time of writing, no other forms of $\theta_1$ have been proposed, and this could form the basis of a future study.

Only a very simple one-step, single-phase reaction model was used in this study. In reality, reaction pathways are extremely complicated, and depending on the chemical species being modeled, this level of simplification may be highly inadequate. For example, Meredith et al. [40] recently simulated the ignition of HMX using a condensed-phase model consisting of two irreversible decomposition pathways and several subphases with different physical properties, and a gas-phase model with 45 species and 231 elementary reaction steps. In principle, the author sees no reason that the GPR model would not cope just as well with these processes as the models used in the cited paper. Transitioning between different phases would mean only varying the strain dissipation time, and perhaps the EOS; a great simplification to the multi-model frameworks typically used.

In Section 4.4 it was demonstrated that the method proposed in Section 3 can be used to significantly reduce the computational time in the heating phase of cookoff simulations on short bounded domains. An example of a real-world setup benefiting from this technique would be the constant-pressure HMX heating experiments of Renlund et al. [47]. Some examples of numerical experiments benefiting from this technique would be the heating phase of the simulations of Kapila, Schwendeman, et al. [34, 53], where the detonation response to different temperature gradients at constant pressure is investigated.

The isobaric cookoff technique is, in a sense, similar to existing techniques used in modeling solid cookoff, where the material is assumed not to flow in the heating phase [43]. The governing system of equations and its method of solution are, however, very different, and these previous models do not transform into a flow model upon detonation. The crucial realization here is that fluid cookoff can be modeled in the same way if the acoustic wave generated by the heating hits bounding wall relatively early and pressure equilibrates over a relatively short period of time.

[5] A Newtonian fluid is one in which the shear rate is directly proportional to the shear stress.

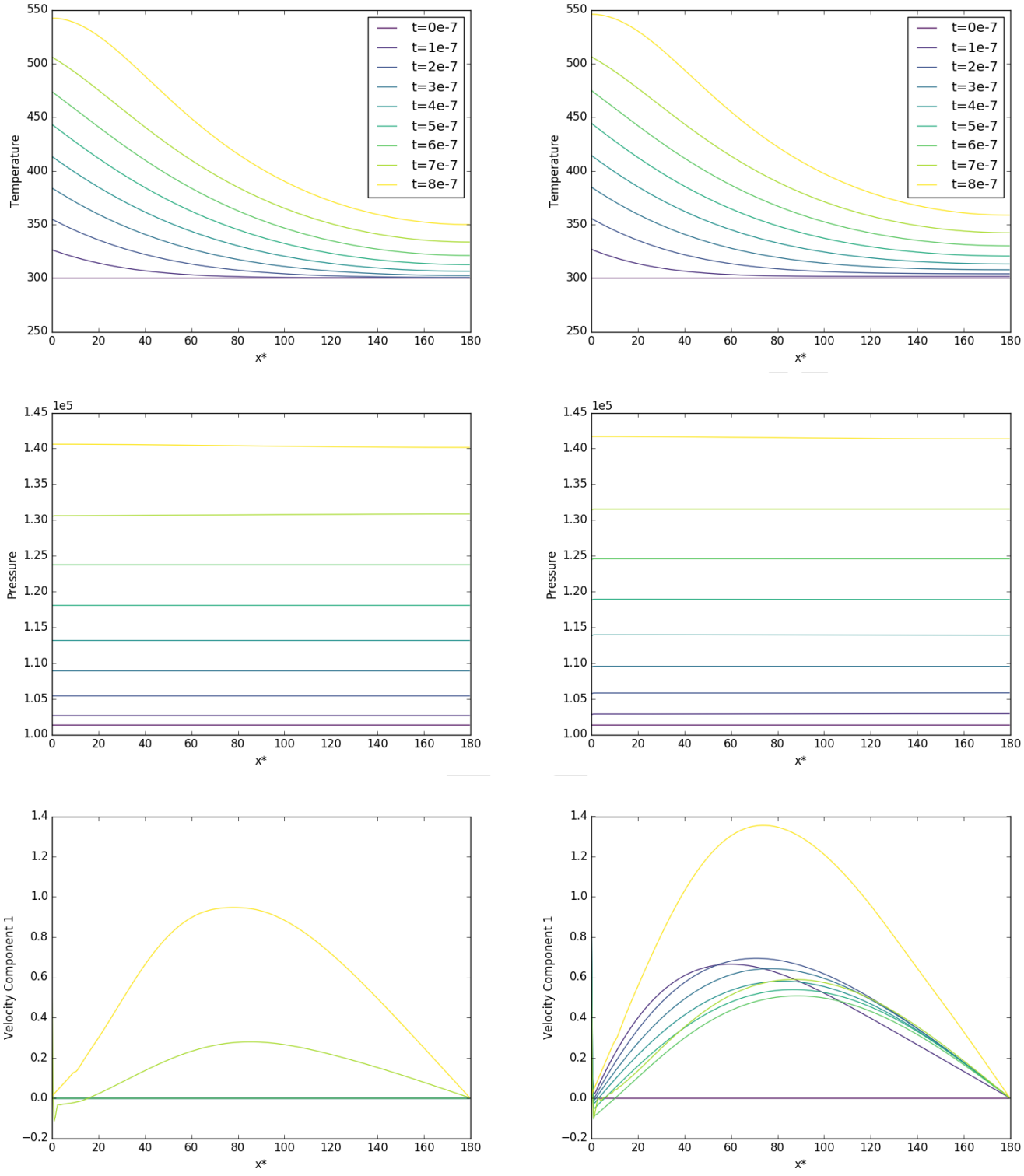


Figure 4: Temperature, pressure, and velocity in the heating phase of the slow cookoff test for the reduced system (left) / full system (right)

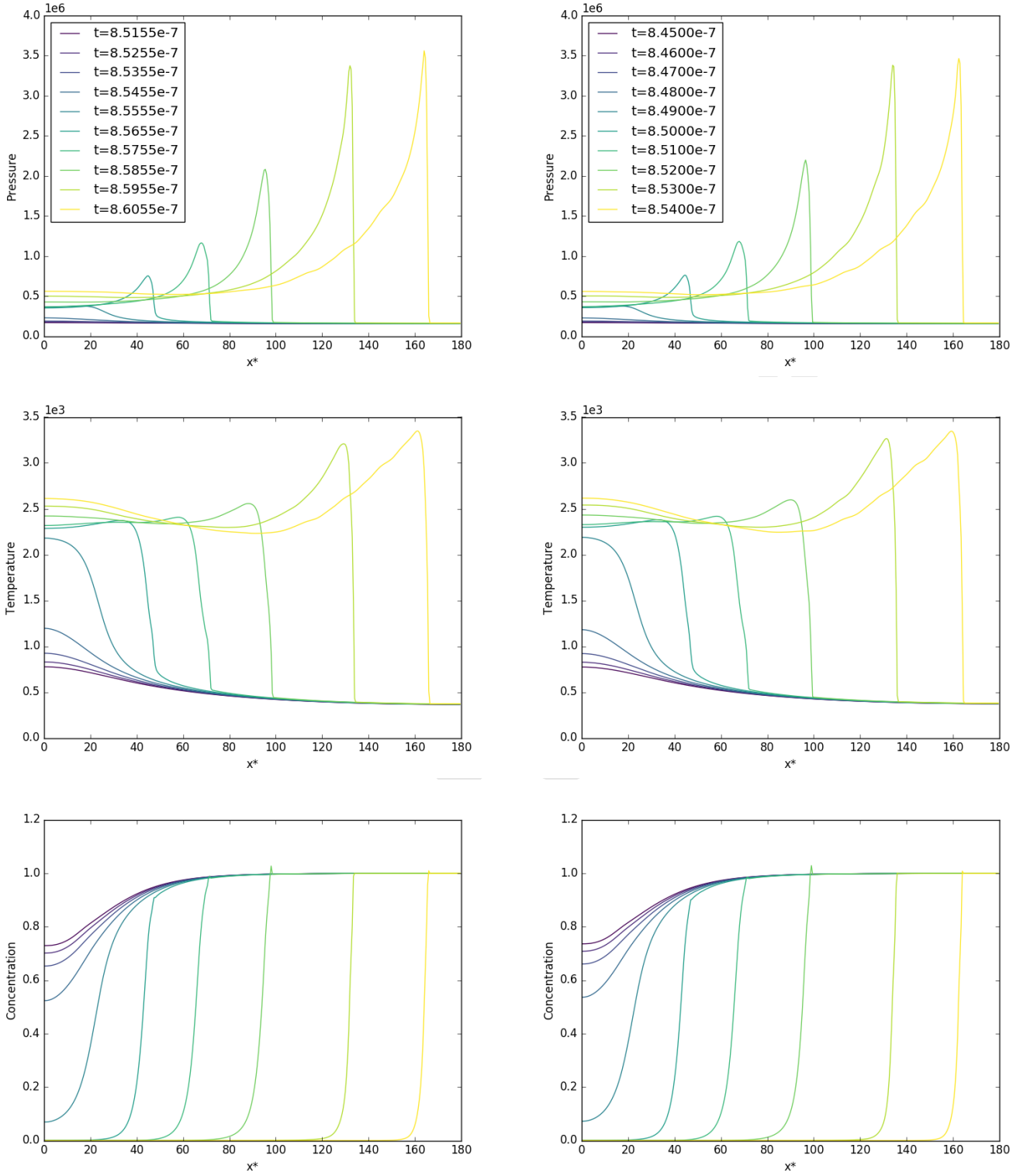


Figure 5: Pressure, temperature, and concentration of reactant in the detonation phase of the slow cookoff test for the reduced system (left) / full system (right)

The isobaric cookoff technique is similar to the mass scaling technique described in 1.1, in that both produce an approximate, explicitly-solved system with a larger time step. Both techniques achieve a similar time step increment. Whilst the mass scaling technique applies not just to constant-pressure flows, the technique here is much more computationally efficient, retains the hyperbolic character of the thermal conduction, and does not produce spurious oscillations in the motions of the heated materials (as the materials are assumed to be motionless while only the reduced system is calculated).

### *5.1. Limitations*

Firstly, all tests were carried out in 1D. Several multidimensional test cases are presented for the GPR model in [17, 9], including the circular explosion problem, the 3D Taylor-Green vortex, and the viscous double Mach reflection problem of Woodward and Colella [61], among others. However, several aspects of combustion are inherently multidimensional phenomena (such as hotspot formation, which can induce inhomogeneities in the profiles of combustion waves [53], or gas intrusions and channeling, which are important in deflagration-to-detonation processes [5]). The GPR model thus far has not been tested with any consideration of these phenomena, and this remains to be done.

The results of Gross et al. [27] suggest that the isobaric cookoff technique would still be applicable to mixtures of fluids, as pressures still tend to equilibrate, but this is a complication that needs to be borne in mind.

The isobaric cookoff technique only works on bounded domains which are relatively short in comparison to the speed of sound in the medium. This is because if the initial acoustic wave generated in the heating process does not reach the end of the domain early on in the simulation, the constant-pressure assumption will not be a realistic approximation to the system, leading to an incorrect calculation of the density (derived from the very accurate calculation of the temperature by the thermal subsystem).

Another problem with the method in its current form is that it assumes that the reactive material is structurally homogeneous. Whilst this may be a fair assumption in some situations for relatively inviscid gases, it is very unlikely to be realistic in many situations involving modeling detonations in solids, where gaps and thermal damage (porosity and cracks) develop over the long heating phase [64]. Inhomogeneities in the reactive materials can lead to very different outcomes, as demonstrated by Schwendeman and Kapila [53].

### *5.2. Potential Improvements*

There are some potential improvements that could be made to the isobaric cookoff technique. Leveque's *Large Time Step Method* [36] may present a further technique to speed up the calculation of the heating phase. This would require solution of the Riemann Problem of the thermal conduction subsystem of the GPR model. This is a relatively simple, conservative hyperbolic system with sources. Whilst there does not appear to be any published exact solutions available, there are a variety of techniques that could be applied to solve a Riemann Problem such as this (see Montecinos et al. for a recent overview [41]).

It may be that larger speed-ups than those demonstrated here could be achieved by the use of an implicit solver for the reduced system, owing to the larger time steps that this would permit. See Clutter [14] for some benchmark tests of explicit and implicit solvers for reactive systems. Implicit-Explicit (IMEX) methods are another technique [7, 6], involving solving the acoustic terms implicitly to avoid the acoustic CFL condition, while solving the advection and conduction terms explicitly, similarly to the method proposed in [38]. The explicit solves could be subcycled (repeated many times for each larger time step of the implicit solver), permitting the use of the larger implicit time steps. IMEX methods would allow the simulation of systems displaying non-constant pressure, acoustic waves, and flow.

Solving the equations at least partly implicitly requires the iterative solution of a non-linear system. This requires more algorithmic machinery and often tailored preconditioners to achieve good convergence speeds. The domain of dependence of the solution becomes the whole domain, in some sense destroying the localized nature of the hyperbolic system (and the associated benefits detailed in 1.2), and making impossible the trivial parallelisation inherent to the original system. This may prove more costly for very large grids, whereas the cost-per-iteration of an explicit solver to the hyperbolic system will not increase substantially, as long as additional computational cores are available. The performance of a method such as this, compared with that proposed in this study, will depend to some extent on both algorithmic, software, and hardware implementations, and benchmarking for the desired usage cases should be performed to decide which is more desirable. It must also be borne in mind that the method proposed in this study is much simpler to implement, and the transition period from the reduced to the full system does not present any of the myriad issues commonly associated with implicit methods, discussed in 1.1.

It was noted in Section 4.4 that the reduced system detonates slightly later than the full system, owing to the fact that the convection of warm material away from the heated left boundary (a process ignored by the reduced system) results in slightly more energy being pumped into the full system, as the boundary is held at a fixed temperature. To ensure that exactly the same amount of energy has entered both systems at each point in time, a fixed flux boundary condition (as described in Section 2.1) could be used. It's important to note, however, that in the rudimentary implementation of this condition presented here, at each time step all the additional thermal energy resulting from the heat flux is added to just one boundary cell. If a very fine grid is used, this will result in very large, nonphysical values for the temperature at the boundary. It may be possible to rectify this problem by smearing out the additional thermal energy at each time step over a layer a few cells thick at the boundary.

Caution must be taken in deciding which proportions of the total additional energy to add to which cells, however, so that a physically-relevant solution is obtained. It may be instructive to obtain some analytical results regarding the depth of penetration of the heat flux over the time step, which would be available for the classical Fourier law of heat conduction in some situations. Alternatively, a subcycle of the thermal conduction system of the GPR model could be perform at the beginning of every time step to determine how far the heat flux penetrates the medium, given the temperature and density distribution around the boundary.

A second-order accurate solver for the GPR model has recently been proposed by Jackson [32]. It has been demonstrated to be 5-15 times faster than the equivalent ADER-WENO method on a variety of problems. Thus, it may be possible to attain this order of speedup in computing the later stages of the cookoff process, when the full GPR system is employed. The method presented in the referenced study relies on an operator splitting, of the kind described in Section 2.2. It would be straightforward to incorporate into this framework the analytical solution (38b) for the time evolution of the reactive species. It is not immediately clear, however, how more complicated reaction dynamics would be integrated into the framework, and this method is unable to provide the arbitrarily high-order solutions that the ADER-WENO method is capable of, which may be important to accurately capture the complex evolution of the phenomena arising in cookoff problems.

## 6. References


[1] *ALE3D*. https://wci.llnl.gov/simulation/computer-codes/ale3d.

[2] *The TOP500 Project*. https://www.top500.org.

[3] S. Arrhenius, *On the Reaction Velocity of the Inversion of Cane Sugar by Acids*, Zeitschrift für Physikalische Chemie, 4 (1889), pp. 226–248.

[4] ———, *The heat of dissociation of electrolytes and the influence of temperature on the degree of dissociation*, Wilhelm Engelmann, 1889.

[5] B. W. Asay, *Non-Shock Initiation of Explosives*, Springer, 2010.

[6] U. M. Ascher, S. J. Ruuth, and R. J. Spiteri, *Implicit-explicit Runge-Kutta methods for time-dependent partial differential equations*, Applied Numerical Mathematics, 25 (1997), pp. 151–167.

[7] U. M. Ascher, S. J. Ruuth, and B. T. R. Wetton, *Implicit-Explicit Methods for Time-Dependent Partial Differential Equations*, SIAM Journal on Numerical Analysis, 32 (1995), pp. 797–823.

[8] F. Bampi and A. Morro, *Viscous Fluids with Hidden Variables and Hyperbolic Systems*, Wave Motion, 2 (1980), pp. 153–157.

[9] W. Boscheri, M. Dumbser, and R. Loubère, *Cell centered direct Arbitrary-Lagrangian-Eulerian ADER-WENO finite volume schemes for nonlinear hyperelasticity*, Computers and Fluids, 134-135 (2016), pp. 111–129.

[10] D. L. Chapman, *On the Rate of Explosion in Gases*, Philosophical Magazine Series 5, 47 (1899), pp. 90–104.

[11] J. F. Clarke, D. R. Kassoy, and N. Riley, *Shocks generated in a confined gas due to rapid heat addition at the boundary*, Proceedings of the Royal Society of London A, 393 (1984), pp. 309–329.

[12] ———, *On the direct initiation of a plane detonation wave*, Proceedings of the Royal Society of London A, 408 (1986), pp. 129–148.

[13] ———, *On the evolution of plane detonations*, Proceedings of the Royal Society of London A, 429 (1990), pp. 259–283.

[14] J. K. Clutter, *Application of Computational Modeling for Explosive Hazard Assessments*, International Journal of Protective Structures, 4 (2013), pp. 293–314.

[15] A. Compte and R. Metzler, *The generalized Cattaneo equation for the description of anomalous transport processes*, Journal of Physics A: Mathematical and General, 30 (1997), pp. 7277–7289.

[16] W. Doring, *On detonation processes in gases*, Annalen der Physik, 43 (1943), pp. 421–436.

[17] M. Dumbser, I. Peshkov, E. Romenski, and O. Zanotti, *High order ADER schemes for a unified first order hyperbolic formulation of continuum mechanics: Viscous heat-conducting fluids and elastic solids*, Journal of Computational Physics, 314 (2016), pp. 824–862.

[18] D. A. Frank-Kamenetskii, *Diffusion and Heat Exchange in Chemical Kinetics*, Princeton University Press, 1955.

[19] J. Frenkel, *Kinetic Theory of Liquids*, Oxford University Press, 1947.

[20] M. Fukuma and Y. Sakatani, *Relativistic Viscoelastic Fluid Mechanics*, International Journal of Modern Physics: Conference Series, 21 (2013), pp. 189–190.

[21] R. Geroch, *Relativistic theories of dissipative fluids*, Journal of Mathematical Physics, 36 (1995), pp. 4226–4241.

[22] S. K. Godunov and E. I. Romenski, *Nonstationary equations of nonlinear elasticity theory in eulerian coordinates*, Journal of Applied Mechanics and Technical Physics, 13 (1974), pp. 868–884.

[23] H. Gomez, I. Colominas, F. Navarrina, and M. Casteleiro, *A finite element formulation for a convection-diffusion equation based on Cattaneo's law*, Computer Methods in Applied Mechanics & Engineering, 196 (2007), pp. 1757–1766.

[24] H. Gomez, I. Colominas, F. Navarrina, J. Pares, and M. Casteleiro, *A hyperbolic theory for advection-diffusion problems: Mathematical foundations and numerical modeling*, Archives of Computational Methods in Engineering, 17 (2010), pp. 191–211.

[25] P. Gresho, *On the theory of semi-implicit projection methods for viscous incompressible flow and its implementation via a finite element method that also introduces a nearly consistent mass matrix. Part 1: Theory*, International Journal for Numerical Methods in Fluids, 11 (1990), pp. 587–620.

[26] ———, *On the theory of semi-implicit projection methods for viscous incompressible flow and its implementation via a finite element method that also introduces a nearly consistent mass matrix. Part 2: Implementation*, International Journal for Numerical Methods in Fluids, 11 (1990), pp. 587–620.

[27] M. L. Gross, K. V. Meredith, and M. W. Beckstead, *Fast cook-off modeling of HMX*, Combustion & Flame, 162 (2015), pp. 3307–3315.

[28] C. Helzel, R. J. Leveque, and G. Warnecke, *A Modified Fractional Step Method for the Accurate Approximation of Detonation Waves*, SIAM Journal on Scientific Computing, 22 (2000), pp. 1489–1510.

[29] A. Hidalgo and M. Dumbser, *ADER schemes for nonlinear systems of stiff advection-diffusion-reaction equations*, Journal of Scientific Computing, 48 (2011), pp. 173–189.

[30] W. M. Howard, M. A. Mcclelland, J. Knap, A. L. Nichols, and L. Livermore, *ALE3D Simulations of Gap Closure and Surface Ignition for Cookoff Modeling*, 13th International Detonation Symposium, (2006).

[31] W. Israel and J. M. Stewart, *Transient relativistic thermodynamics and kinetic theory*, Annals of Physics, 118 (1979), pp. 341–372.

[32] H. Jackson, *A Fast Numerical Scheme for the Godunov-Peshkov-Romenski Model of Continuum Mechanics*, (2017).

[33] E. Jouget, *On the Propagation of Chemical Reactions in Gases*, Journal de Mathématiques Pures et Appliquées, 1 (1905), pp. 347–425.

[34] A. Kapila, D. W. Schwendeman, J. J. Quirk, and T. Hawa, *Mechanisms of detonation formation due to a temperature gradient*, Combustion Theory & Modelling, 6 (2002), pp. 553–594.

[35] S. A. Khairallah and A. Anderson, *Mesoscopic simulation model of selective laser melting of stainless steel powder*, Journal of Materials Processing Technology, 214 (2014), pp. 2627–2636.

[36] R. J. Leveque, *A Large Time Step Generalization of Godunov ' s Method for Systems of Conservation Laws*, SIAM Journal on Numerical Analysis, 22 (1985), pp. 1051–1073.

[37] A. N. Malyshev and E. I. Romenskii, *Hyperbolic equations for heat transfer. Global solvability of the Cauchy problem*, Siberian Mathematical Journal, 27 (1986), pp. 734–740.

[38] R. Mccallen, T. Dunn, A. Nichols, and J. Reaugh, *Modeling of Thermal Convection of Liquid TNT for Cookoff*, Proceedings of the NECDC 2002, (2003).

[39] M. A. McClelland, E. A. Glascoe, A. L. Nichols, S. P. Schofield, and

H. K. Springer, *ALE3D Simulation of Incompressible Flow, Heat Transfer, and Chemical Decomposition of Comp B in Slow Cookoff Experiments*, 15th International Detonation Symposium, (2014).

[40] K. V. Meredith, M. L. Gross, and M. W. Beckstead, *Laser-induced ignition modeling of HMX*, Combustion & Flame, 162 (2015), pp. 506–515.

[41] G. Montecinos, C. E. Castro, M. Dumbser, and E. F. Toro, *Comparison of solvers for the generalized Riemann problem for hyperbolic systems with source terms*, Journal of Computational Physics, 231 (2012), pp. 6472–6494.

[42] G. I. Montecinos, L. O. Müller, and E. F. Toro, *Hyperbolic reformulation of a 1D viscoelastic blood flow model and ADER finite volume schemes*, Journal of Computational Physics, 266 (2014), pp. 101–123.

[43] A. L. Nichols and S. Schofield, *Modeling the Response of Fluid / Melt Explosives to Slow Cook-Off*, 15th International Detonation Symposium, (2014).

[44] H. Nishikawa, *A first-order system approach for diffusion equation. II: Unification of advection and diffusion*, Journal of Computational Physics, 229 (2010), pp. 3989–4016.

[45] I. Peshkov and E. Romenski, *A hyperbolic model for viscous Newtonian flows*, Continuum Mechanics and Thermodynamics, 28 (2016), pp. 85–104.

[46] A. Prior, *Applications of implicit and explicit finite element techniques to metal forming*, Journal of Materials Processing Technology, 45 (1994), pp. 649–656.

[47] A. M. Renlund, J. C. Miller, W. M. Trott, K. L. Erickson, M. L. Hobbs, R. G. Schmitt, G. W. Wellman, and M. R. Baer, *Characterization of Thermally Degraded Energetic Materials*, tech. rep., Sandia National Laboratories, 1997.

[48] R. D. Ritchtmyer, *Difference methods for initial-value problems*, Interscience, 1957.

[49] P. Romatschke, *New Developments in Relativistic Viscous Hydrodynamics*, International Journal of Modern Physics E, 19 (2010), pp. 1–53.

[50] E. Romenski, D. Drikakis, and E. Toro, *Conservative models and numerical methods for compressible two-phase flow*, Journal of Scientific Computing, 42 (2010), pp. 68–95.

[51] E. Romenski, A. D. Resnyansky, and E. F. Toro, *Conservative hyperbolic model for compressible two-phase flow with different phase pressures and temperatures*, Quarterly of applied mathematics, 65(2) (2007), pp. 259–279.

[52] E. I. Romenski, *Hyperbolic equations of Maxwell's nonlinear model of elastoplastic heat-conducting media*, Siberian Mathematical Journal, 30 (1989), pp. 606–625.

[53] D. W. Schwendeman and A. K. Kapila, *Effect of Thermal Nonhomogeneity on Explosion or Detonation in an Annular Cookoff*, 12th International Detonation Symposium, (2002), pp. 1–11.

[54] J. Selesovský, *Thermal loading of explosives–finite difference method with time step reduction.*, Journal of Hazardous Materials, 174 (2010), pp. 289–94.

[55] M. Short, *On the Critical Conditions for the Initiation of a Detonation in a Nonuniformly Perturbed Reactive Fluid*, SIAM Journal on Applied Mathematics, 57 (1997), pp. 1242–1280.

[56] M. Sućeska and S. Matečić-Mušanić, *Numerical Modeling of Self-Ignition of Energetic Materials*, Central European Journal of Energetic Materials, 1 (2004), pp. 23–41.

[57] V. A. Titarev, E. Romenski, and E. F. Toro, *MUSTA-type upwind fluxes for non-linear elasticity*, International Journal for Numerical Methods in Engineering, 73 (2008), pp. 897–926.

[58] E. Toro, *Riemann solvers and numerical methods for fluid dynamics: a practical introduction*, Springer, 2009.

[59] E. F. Toro, *On Glimm-Related Schemes for Conservation Laws*, Preprint MMU-9602, Department of Mathematics & Physics, Manchester Metropolitan University, UK, (1996).

[60] J. von Neumann, *Theory of Detonation Waves*, tech. rep., Institute for Advanced Study, 1942.

[61] P. Woodward, *The Numerical Simulation of Two-Dimensional Fluid Flow with Strong Shocks*, Journal of Computational Physics, 54 (1984), pp. 115–173.

[62] V. Yakhot, *A New Approach to Modelling Strongly Non-Equilibrium, Time-Dependent Turbulent Flows*, tech. rep., Institute for Advanced Study, 2003.

[63] J. J. Yoh, *Simulating the Thermal Response of High Explosives on Time Scales of Days to Microseconds*, AIP Conference Proceedings, (2004), pp. 425–428.

[64] J. J. Yoh, M. A. Mcclelland, J. L. Maienschein, L. Nichols, and J. F. Wardell, *Towards An Ideal Slow Cookoff Model For PBXN-109*, JANNAF 2003 Conference Proceedings, (2003).

[65] J. J. Yoh, M. A. Mcclelland, J. L. Maienschein, and J. F. Wardell, *Towards a predictive thermal explosion model for energetic materials*, Journal of Computer-Aided Materials Design, 10 (2003), pp. 175–189.

[66] Y. B. Zeldovich, *On the Theory of the Propagation of Detonation in Gaseous Systems*, Journal of Experimental & Theoretical Physics, 10 (1940), pp. 542–568.